Online compressed sensing MR image reconstruction for high resolution T_2^* imaging

L. El Gueddari,[1,2] E. Chouzenoux,[3,4] A. Vignaud,[1] and J.-C. Pesquet,[3,4] Ph. Ciuciu,[1,2,*]

[1]CEA/NeuroSpin, Univ. Paris-Saclay, Gif-sur-Yvette, France

Inria Saclay-Ile de France, Parietal, France

[3]Inria Saclay-Ile de France, Opis, Palaiseau, France

[4]CentraleSupélec, CVN, Gif-sur-Yvette, France

[*]To whom correspondence should be addressed; E-mail: philippe.ciuciu@cea.fr.

May, 14 2019

Abstract

Compressed sensing theory reduces lengthy acquisition time in MRI at the expense of computationally demanding iterative reconstruction. Usually, reconstruction is performed *offline* once all the data have been collected. Here, we introduce an online CS reconstruction framework that interleaves acquisition and reconstruction steps in a convex setting and permits the delivery of intermediate images on the scanner console during acquisition. In particular, the sum of acquisition and reconstruction times is reduced without compromising image quality. The gain of this strategy is shown both on retrospective Cartesian and prospective non-Cartesian under-sampled ex-vivo baboon brain data at 7T with an in-plane resolution of 400μm.

Introduction

Magnetic resonance imaging has proved it versatility to probe soft tissues, especially it addresses a large set of contrast that brings complementary information on the underlying organ to facilitate diagnosis. However acquisition in MRI is slow in particular when in comes to T2*-weighted images in a high resolution context. Compressed Sensing (CS) theory tackle this issue at the expense of complex and slow reconstruction. In this work we proposed a new framework

where acquisition and reconstruction are interleaved, it is based on a batch formulation of the reconstruction problem that allows to reduce the overall acquisition and reconstruction time. Therefore a partial solution could be given during acquisition. This new reconstruction framework is compatible with a Gadgetron (*1*) formulation, which leads to clinical use of Compressed Sensing.

Theory

Problem statement. Let us first define the offline reconstruction problem solved in CS. Let N, S, C and $\boldsymbol{x}$ being respectively the image dimension, number of shots used to acquire the NMR signal ($\boldsymbol{y} \in \mathbb{C}^{CS}$), the number of shots and the recovered image. $\boldsymbol{T}$ will define a Wavelet Transform (*2*). The offline reconstruction problem reads as follows:

$$\hat{\boldsymbol{x}} = \underset{\boldsymbol{x}\in\mathbb{C}^N}{\operatorname{argmin}} \left\{ \frac{1}{2} \| f_\Omega(\boldsymbol{x}) - \boldsymbol{y}_\Omega \|_{\mathrm{F}}^2 + \lambda_1 \| \boldsymbol{T}\boldsymbol{x} \|_1 \right\} \tag{1}$$

For an online implementation of CS reconstruction, we introduce n_b the number of batches and s_b the number of shots per batch and n_j the number of iteration per batch. The k-space support of the j^{th}-batch will be defined as $\Omega_j = \cup_{0\leq j\leq n_b} \Gamma_i$ where Γ_i is the i^{th} shot support. The online reconstruction reads as follows:

$$\forall j \in \mathbb{N}, 0\ leqi \leq n_b,\ \hat{\boldsymbol{x}}^j = \underset{\boldsymbol{x}\in\mathbb{C}^N}{\operatorname{argmin}} \left\{ \frac{1}{2} \frac{1}{\#\Omega_j} \| f_{\Omega_j}(\boldsymbol{x}) - \boldsymbol{y}_{\Omega_j} \|_{\mathrm{F}}^2 + \lambda_2 \| \boldsymbol{T}\boldsymbol{x} \|_1 \right\} \tag{2}$$

λ_1 and λ_2 controls the sparsity level. The two formulation are equivalent for $\lambda_2 = \lambda_1/\#\Omega_{n_b}$. Each newly available batch has to be taken into account, this leads to the following constraint on the number of iteration per batch:

$$\forall j \in \mathbb{N}, 0 < j \leq n_b - 1,\ n_j \times T_{it} \approx s_b \times \mathrm{TR} \tag{3}$$

To ensure convergence, the last batch will have a number of iteration large enough. In terms of optimization, we implemented a primal-dual (*3, 4*) optimization summarized in Fig. 1

Results

Parameters setting. A T2*-weighted ex-vivo baboon brain was acquired on a 7T system with in-plane resolution of 400μm and 3mm slice thickness, a FOV of 20.4cm, a base resolution of 512×512. The acquisition parameters were set as follows: TR=550ms (for 11 slices), TE=30ms and FA=25°. The decimated bi-Orthogonal Wavelet Transform with 4 decomposition scale was used as sparsifying transform and λ_2 was set retrospectively. All experiments were run on a machine with 128 GB of RAM and an 8-core (2.40 GHz) Intel Xeon E5-2630 v3 Processor and the code have been developed in python using PySAP package.

Retrospective Cartesian sampling The sampling mask composed of 187 lines of 512 samples is illustrated Fig .2. The 12 central line were collected first while the others are acquired in a pseudo-random order. We used the FFT, in this set-up, $T_{it} = 0.12s$. The batch size was tested over a discrete sets of value, $s_b = 2, 23, 46$ and 92 shots/batch. The evolution of the performance of the reconstruction was evaluated thanks to the SSIM index (*5*). The results are illustrated Fig. 3 **(a)**, and Fig. 2 represent the reconstruction by the end of acquisition i.e. at 92s.

Prospective non-Cartesian sampling A modified 2D T2*-weighted GRE sequence was implemented based on the multi-shot Sparkling trajectories (*6*) with $S = 43$ and $C = 3072$, an acceleration factor of 12 in time and an under-sampling factor of 0.55. The sequence was implemented using a golden angle strategy(i.e. $\approx 130°$ between two shots) and the NFFT (*7*) was used. In this setting, $T_{it} = 0.25s$, hence $n_k = s_b \times 2$. The sets of batch size parameters are summarized Table 1. The evolution of the SSIM score is given Fig. 3 **(b)**, and Fig. 4 represents the reconstruction at the end of the acquisition (i.e. at 21.5s from the beginning of the acquisition). Despite the slowness of the NFFT, the gain is significant.

Conclusion & Discussion

In this work we proposed a framework for online reconstruction from segmented under-sampled data. We demonstrate its advantages and application to T2*-weighted high-resolution 2D imaging both on Cartesian and non-Cartesian sampling schemes. In terms of reconstrcution, the proposed method converges to the same image as the offline solution. Additionally this approach delivers a reliable intermediate MR image during acqisition. This new reconstruction framework is compatible with the Gadgetron (*1*) implementation, which makes it appealing for clinical use of CS in daily routine.

Figures

Table 1: Setting of online reconstruction parameters.

	Batch size s_b	Iterations n_j	Number of iterations n_b
Offline	[43]	[200]	1
H1	[5, 15, 29, 43]	[22, 30, 30, 200]	4
H2	[7, 14, 21, 28, 35, 43]	[15, 15, 15, 15, 17, 200]	6
H3	[4, 8, 12, ..., 40, 43]	[8, 8, 8, ..., 8, 6, 200]	11

References and Notes

1. M. Hansen and T. Srensen, "Gadgetron: An open source framework for medical image reconstruction," *Magnetic Resonance in Medicine*, vol. 69, no. 6, pp. 1768–1776, 2013.

2. I. Daubechies, "The wavelet transform, time-frequency localization and signal analysis," *IEEE transactions on information theory*, vol. 36, no. 5, pp. 961–1005, 1990.

3. B. Vũ, "A splitting algorithm for dual monotone inclusions involving cocoercive operators," *Advances in Computational Mathematics*, vol. 38, no. 3, pp. 667–681, Apr 2013.

Algorithm 1: Condat-Vú algorithm

initialize $i = 1, j = 1, \boldsymbol{x}_1^1, \boldsymbol{z}_1^1$;
while $j \leq n_b$ **do**
  $\kappa_j := \frac{\beta_j}{2\|\boldsymbol{T}\|^2}$;
  $\tau_j := \frac{1}{\beta_j}$;
  while $i \leq n_j$ **do**
    $\boldsymbol{x}_{i+1}^j := \boldsymbol{x}_i^j - \tau_j \left(\nabla f_{\Omega_j}(\boldsymbol{x}_i^j) + \boldsymbol{T}^* \boldsymbol{z}_i^j \right)$;
    $\boldsymbol{w}_{i+1}^j := \boldsymbol{z}_i^j + \kappa_j \boldsymbol{T} \left(2\boldsymbol{x}_{i+1}^j - \boldsymbol{x}_i^j \right)$;
    $\boldsymbol{z}_{i+1}^j := \boldsymbol{w}_{i+1}^j - \kappa_j \, \text{prox}_{g/\kappa_j} \left(\frac{\boldsymbol{w}_{i+1}^j}{\kappa_j} \right)$;
    $i := i + 1$;
  end
  $\boldsymbol{x}_1^{j+1} := \boldsymbol{x}_{n_k}^j$;
  $\boldsymbol{z}_1^{j+1} := \boldsymbol{z}_{n_k}^j$;
  $j := j + 1$;
end

Figure 1: Adaptation of the Condat-Vú (*3, 8*) sequence for online reconstruction. $\boldsymbol{z} = \boldsymbol{T}\boldsymbol{x}$, and the hyper-parameters are set line **3.** and **4.** with β_j the Lipschitz constant of the spectral norm of f_{Ω_j}: $\beta_j = \|f_{\Omega_j}\|^2$. In practice for Cartesian case $\forall j \in \mathbb{N}, 1 \leq j \leq n_b, \|f_{\Omega_j}\|^2 = 1$ and for non-Cartesian case, we will evaluate the norm using the power iteration method (*9*).

4. L. Condat, "A primal–dual splitting method for convex optimization involving lipschitzian, proximable and linear composite terms," *Journal of Optimization Theory and Applications*, vol. 158, no. 2, pp. 460–479, Aug 2013.

5. Z. Wang, A. Bovik, H. Sheikh, and E. Simoncelli, "Image quality assessment: from error visibility to structural similarity," *IEEE transactions on Image Processing*, vol. 13, no. 4, pp. 600–612, 2004.

6. C. Lazarus, P. Weiss, N. Chauffert, F. Mauconduit, L. El Gueddari, C. Destrieux, I. Zemmoura, A. Vignaud, and P. Ciuciu, "Variable-density k-space filling curves for accelerated Magnetic Resonance Imaging," 2018.

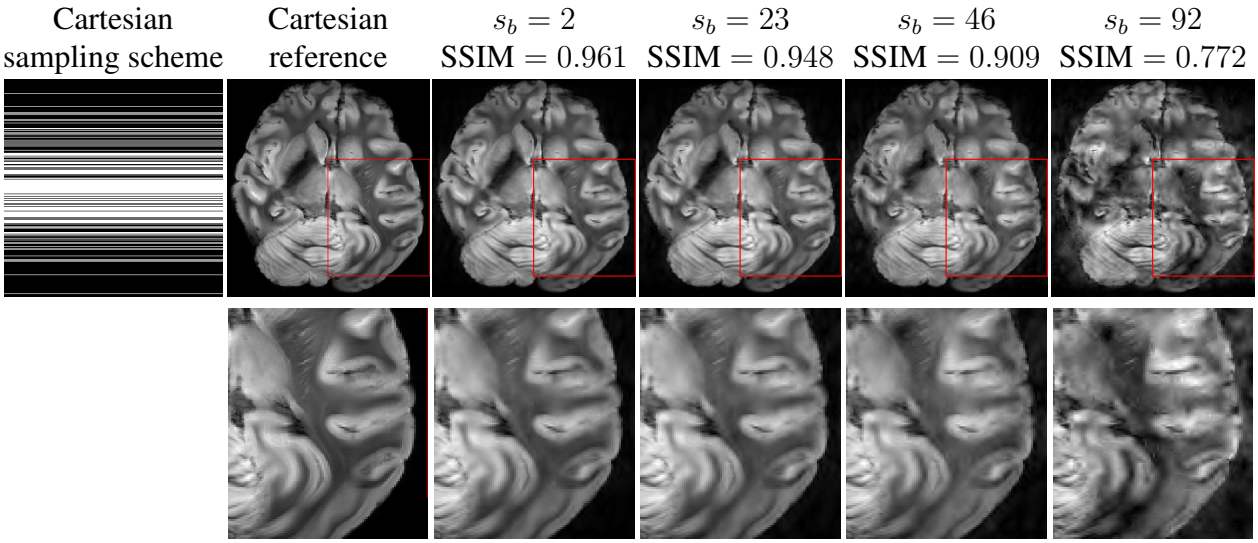

Figure 2: Online reconstructed Cartesian MR images(top) and their respective zooms (bottom) at the end of the acquisiion and for different batch sizes.

7. J. Keiner, S. Kunis, and D. Potts, "Using NFFT 3—a software library for various nonequispaced fast fourier transforms," *ACM Transactions on Mathematical Software (TOMS)*, vol. 36, no. 4, pp. 19, 2009.

8. L. Condat, "A primal–dual splitting method for convex optimization involving Lipschitzian, proximable and linear composite terms," *Journal of Optimization Theory and Applications*, vol. 158, no. 2, pp. 460–479, 2013.

9. W. Press, S. Teukolsky, W. Vetterling, and B. Flannery, *Numerical Recipes 3rd Edition: The Art of Scientific Computing*, Cambridge University Press, New York, NY, USA, 3 edition, 2007.

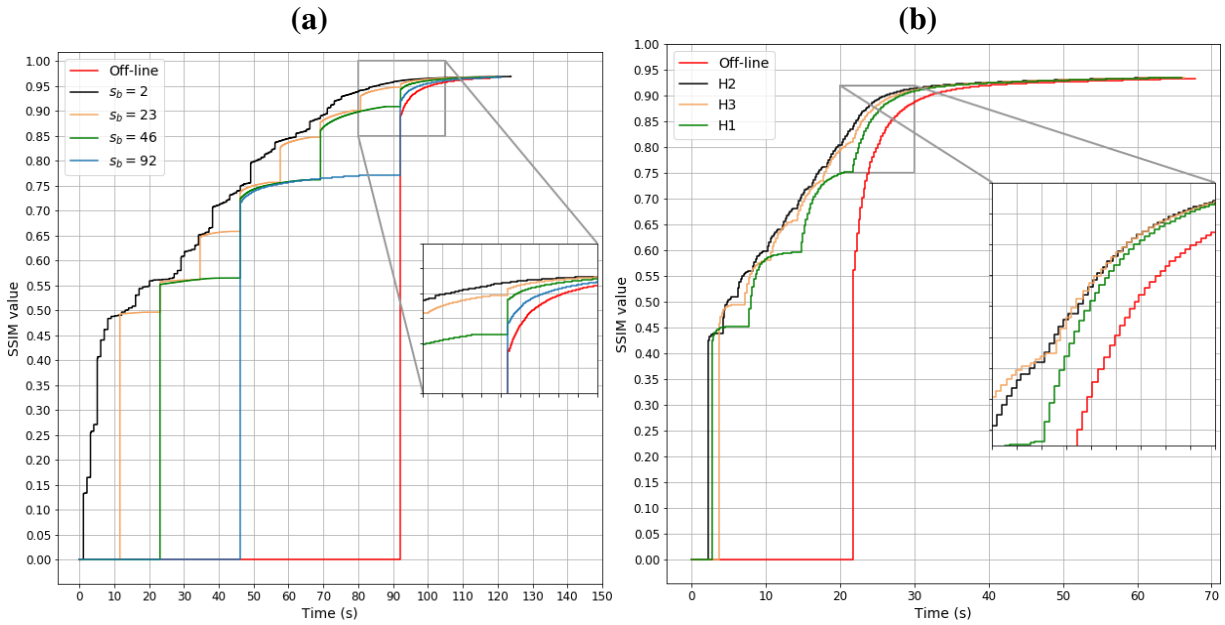

Figure 3: **(a)** Evolutaion of the SSIM score for the diferent batch size on the retrospective Cartesian data. **(b)** Evolution of the SSIM score for the differents hyper-parameters set-up on prospective non-Cartesian data.

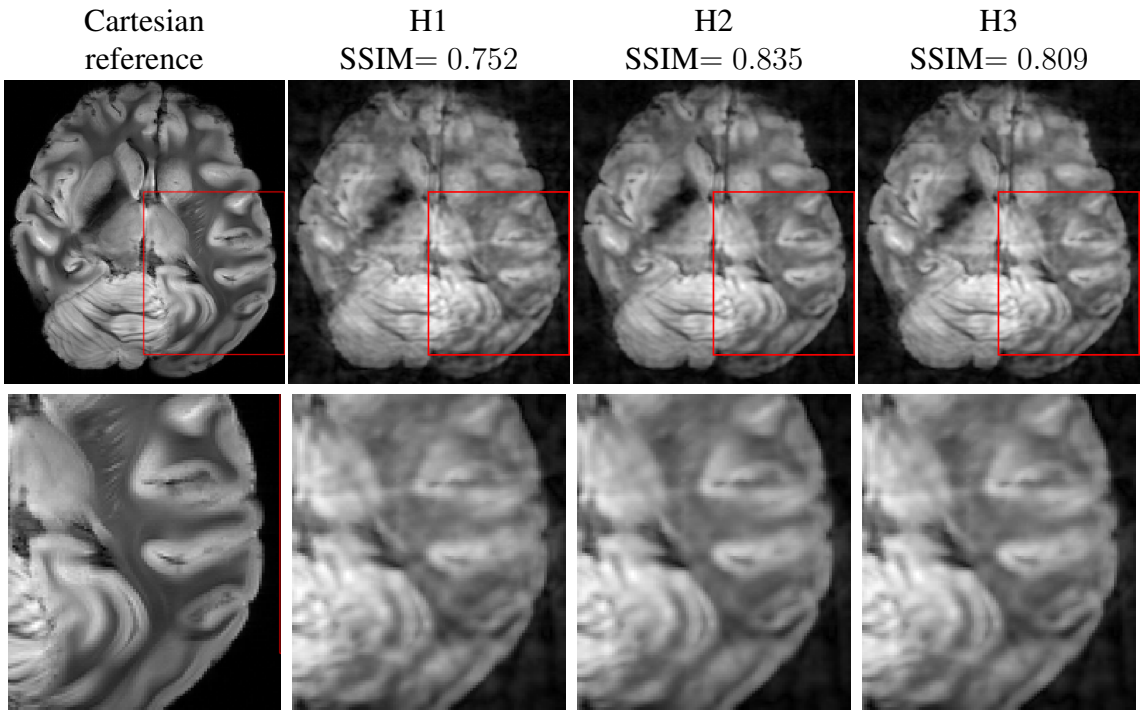

Figure 4: Partial solution obtained at the end of the acquisition (t=21.5s form the begining of the acquisition) and their respective zoom